

Light-Activatable Prodrug and AIEgen Copolymer Nanoparticle for Dual-Drug Monitoring and Combination Therapy

Peng Wu,^{†,‡,∇} Xuefeng Wang,^{§,∇} Zigui Wang,^{‡,||} Wen Ma,[⊥] Jinshan Guo,[#] Jianjun Chen,[⊥] Zhiqiang Yu,^{*,⊥} Jizhen Li,^{*,†} and Dongfang Zhou^{*,‡,⊥}

[†]College of Chemistry, Jilin University, 2519 Jiefang Road, Changchun 130023, P. R. China

[‡]State Key Laboratory of Polymer Physics and Chemistry, Changchun Institute of Applied Chemistry, Chinese Academy of Sciences, Changchun 130022, P. R. China

[§]Department of Obstetrics and Gynecology, Zhujiang Hospital, Southern Medical University, Guangzhou 510282, P. R. China

^{||}School of Applied Chemistry and Engineering, University of Science and Technology of China, Hefei 230026, P. R. China

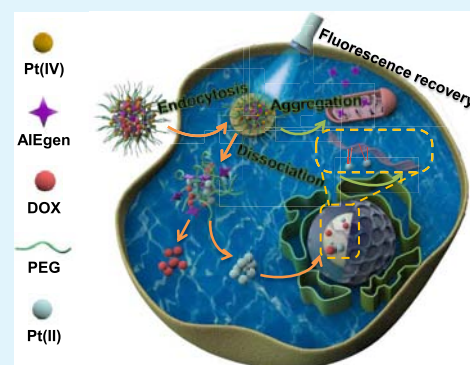
[⊥]Guangdong Provincial Key Laboratory of New Drug Screening, School of Pharmaceutical Sciences, Southern Medical University, Guangzhou 510515, P. R. China

[#]Department of Biomedical Engineering, Pennsylvania State University, University Park, Pennsylvania 16802, United States

Supporting Information

ABSTRACT: Polyprodrug nanoparticles have been employed recently for safer and more effective cancer treatment. However, it remains a challenge to elucidate how and when the polyprodrug nanoparticles are dissociated and activated to release active drugs in cancer cells. Herein, a visible light-activatable Pt(IV) prodrug and an aggregation-induced emission luminogen (AIEgen) were copolymerized and embedded in the main chain of PtAIECP, and the chemotherapeutic doxorubicin (DOX) was subsequently encapsulated in the nanoparticles self-assembled by PtAIECP (PtAIECP@DOX NP). PtAIECP@DOX NP enabled the monitoring of both the light-activation of Pt(IV) prodrug to active Pt(II) and release of encapsulated DOX intracellularly through the fluorescence “turn-on” in the course of visible-light-induced polymer-main-chain cleavage and self-assembled structure dissociation *in vitro* and *ex vivo*. The synergistic anticancer efficacy of the activated Pt(II) drug and DOX in PtAIECP@DOX NP was also investigated *in vitro* and *in vivo*. The implementation of polyprodrug and AIE combination strategy empowered dual drug release and monitoring, which could be further used to guide the temporal and spatial control of light irradiation to maximize therapeutic efficiency, and will inspire other combinational bioimaging and therapy strategies.

KEYWORDS: platinum, AIE, polyprodrug, combination therapy, drug monitoring



1. INTRODUCTION

Polymeric drug delivery systems (PDDSs) have received increasing attention due to prolonged blood circulation, desirable water solubility, and low toxicity.^{1–3} However, current PDDSs are largely based on the encapsulation of chemotherapeutic drugs.^{4–6} The uncontrollable drug release in these systems, to be specific, premature burst release during circulation, and slow diffusional release after accumulation at the tumor site readily led to side effects and yet limited therapeutic efficiency.^{7–11} Polyprodrug nanoparticles with prodrug molecules imbedded into the polymeric backbone have been employed recently for a safer and more effective cancer treatment.^{12–20} Unlike traditional PDDSs, polyprodrug nanoparticles are inactive and stable under normal conditions but can release intact drugs in response to stimuli^{8–11} such as light,^{12–16} redox,^{17–19} or enzymes,²⁰ thus providing better control on drug release and resulting in less side effects. However, it remains a challenge to elucidate how and when the

polyprodrug nanoparticles are dissociated and activated to release active drugs in cancer cells. Given that drug action duration, targeting, and drug accumulation amount in lesion site directly affect the therapeutic effect during cancer treatment,²¹ it is paramount to design a polyprodrug nanoparticle-based system possessing not only precise control on active drug release behavior but also intrinsic ability to monitor prodrug localization and activation to guide the light-irradiation process and to maximize therapeutic efficiency.

Fluorescence molecules can be used for constructing fluorescent nanoprobes.^{22–26} However, traditional dyes suffer from aggregation-caused quenching (ACQ) when they are assembled into nanoparticles.^{27,28} Different from traditional fluorescent dyes, aggregation-induced emission luminogens

Received: February 8, 2019

Accepted: April 30, 2019

Published: April 30, 2019

Scheme 1. Schematic Illustration of a DOX-Loaded Light-Activatable Pt(IV) Prodrug and AIEgen TPE Copolymer Nanoparticle System for Dual-Drug Monitoring and Combination Therapy



(AIEgens) based bioprobes have shown their attractive characteristics for monitoring cellular molecules.^{29–33} Recently, AIEgens were polymerized into polymer backbone to develop AIE polymeric nanoparticles for gene/drug delivery.^{34,35} However, due to the restriction of intramolecular motion mechanism of AIEgens, the fluorescence of the AIEgen polymeric nanoparticles is “always on”.^{36,37} To obtain AIEgen polymeric nanoparticles in situ “turn-on” at application site, complicated molecular design and modification have to be involved.^{38,39}

Recently, we have developed a series of Pt(IV) prodrug-backboned polymers that could be triggered to breakdown in a chain-shattering manner by intracellular reductive agents or remote mild light irradiation to release the active Pt(II) drug.^{15–18} In chemotherapy, the use of a single drug often fails to eradicate tumors due to drug resistance.^{39–43} Herein, we designed a DOX-loaded visible-light-activatable Pt(IV) prodrug and AIEgen tetraphenylethene (TPE) copolymer nanoparticle (PtAIECP@DOX NP) system for dual-drug monitoring and combination therapy. PtAIECP@DOX NP is expected to be able to monitor the light activation of the Pt(IV) prodrug to active Pt(II) and the release of encapsulated DOX simultaneously through the turn-on of dual-color fluorescence. When PtAIECP@DOX NP is intact, due to the fluorescence resonance energy transfer (FRET) between DOX and TPE and the ACQ of DOX, only very weak fluorescence of DOX could be detected. But once PtAIECP@DOX NP is dissociated under the light during the light activation of Pt(IV) into Pt(II), TPE and DOX are released and separated, and the strong fluorescence is restored (Scheme 1). Finally, the combinational anticancer efficacy of the light-activated Pt(II) drug and dissociation-released DOX was evaluated in vitro and in vivo.

2. EXPERIMENTAL SECTION

2.1. Materials and Measurements. Materials and measurements are described in detail in the [Supporting Information](#).

2.2. Synthesis of Pt(IV) and TPE-N. Synthesis and characterization of Pt(IV) and TPE-N are described in detail in the [Supporting Information](#).

2.3. Synthesis of PtAIECP and Preparation of PtAIECP@DOX NP. Pt(IV) (100 mg, 0.245 mmol) was dissolved in dried dimethylformamide (DMF) (1.5 mL), and lysine diisocyanate

(LDI) (100.76 mg, 0.515 mmol) in dried DMF (1 mL) was added dropwise under vigorous stirring; the reaction mixture was allowed to react. TPE-N (155 mg, 0.275 mmol) in dried DMF (2 mL) was then added dropwise under ice bath. After reacting 24 h at room temperature, alkyne-terminated PEG_{2k} (410 mg, 0.205 mmol) in DMF solution (2 mL) was added quickly and the solution was stirred for another 24 h. The final solution was dialyzed against distilled water (MWCO = 3500) for 48 h to remove unreacted monomers and DMF; then, the obtained solution was freeze-dried to give the copolymer PtAIECP.

The above-synthesized PtAIECP was further used to encapsulate DOX. The weight ratio of PtAIECP/DOX-HCl was fixed to 5:1. In detail, PtAIECP (100 mg) was dissolved in dimethyl sulfoxide (DMSO) (2 mL). DOX-HCl (20 mg) was also dissolved in DMSO (2 mL) with the help of triethylamine (3 μ L) to remove HCl. Then, those two solutions were mixed and stirred for another 3 h. The final solution was dialyzed against distilled water (MWCO = 1000) for 48 h to remove unpackage DOX and DMSO and then freeze-dried to obtain PtAIECP@DOX NP. The determination of DOX-loading content is described in detail in the [Supporting Information](#) according to previous ref 44.

2.4. Light Responsiveness. Aqueous solutions of PtAIECP@DOX NP were irradiated under different wavelengths (365, 430, 500 nm, 20 mW/cm²) for preset durations. The change of UV–vis spectra was recorded to check the light responsiveness of PtAIECP@DOX NP. The NP size change was monitored in time by dynamic light scattering (DLS), and the morphology change was observed using transmission electron microscopy (TEM).

2.5. Light-Triggered Drug Release. Light-triggered drug release experiments are described in detail in the [Supporting Information](#) according to previous refs 15, 16, 45.

2.6. Cell Culture. Ovarian cancer cell line Skov3 cells and Skov3/RFP cells (overexpressed red fluorescence protein) were cultured with Gibco1640 (10% fetal bovine serum, 5% CO₂ at 37 °C).⁴⁶

2.7. Cellular Uptake. Skov3 cells were placed into a 6-well culture dish (5 \times 10⁴ cells per well) and cultured overnight. The cells were treated with PtAIECP@DOX NP (20 μ g/mL) for 2 h at 37 °C and divided into two groups. One group was exposed to irradiation (500 nm, 20 mW/cm²) for 30 min and the other group was kept under dark. The cell samples were then washed with phosphate buffered saline (PBS) (pH 7.4) three times, followed by pancreatin digestion and quantitative determination using flow cytometry. For confocal laser scanning microscopy (CLSM) test, endo-/lysosomes of the cells were stained with LysoTracker Red for 30 min at 37 °C. Then, the samples were washed with preheated PBS three times, followed by fixing with 4% formaldehyde for 30 min under dark. For the determination of cellular Pt uptake, the cell samples were washed with

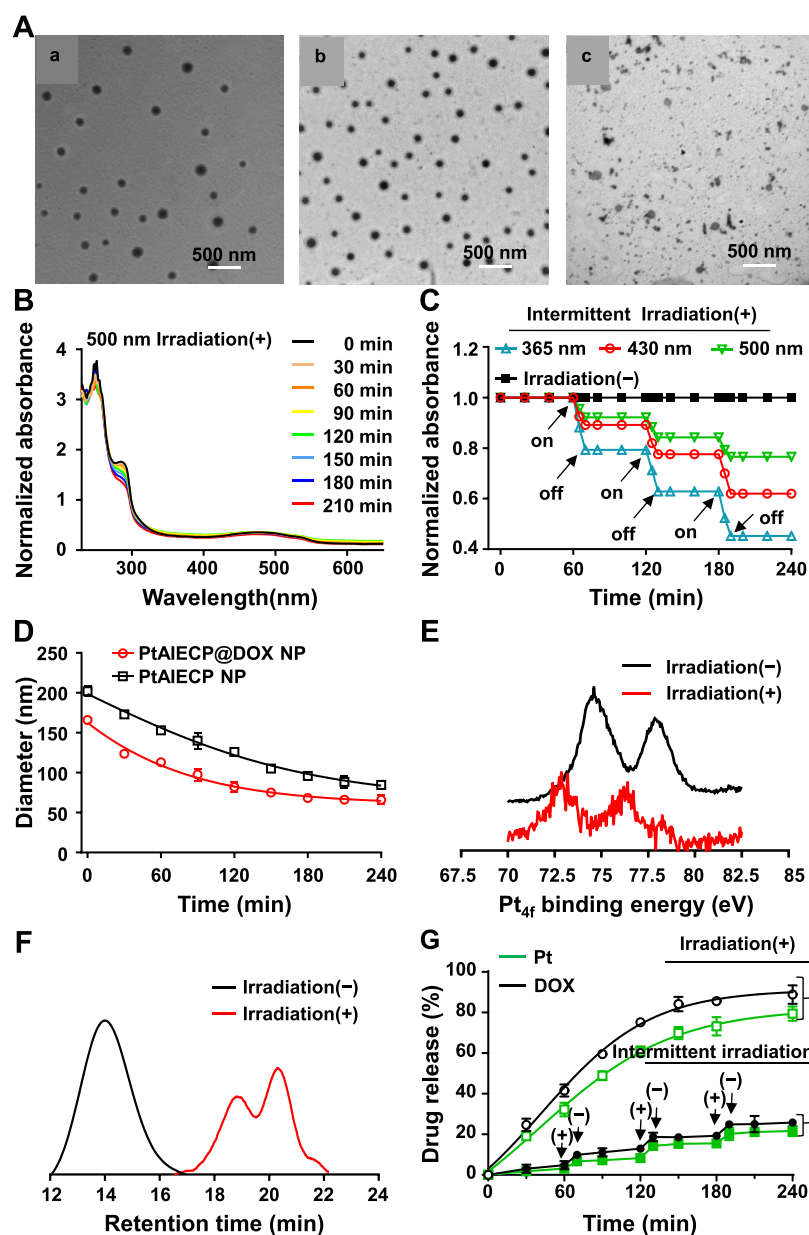


Figure 1. Light activation of PtAIECP NP and PtAIECP@DOX NP. (A) TEM images of (a) PtAIECP NP, (b) PtAIECP@DOX NP, and (c) PtAIECP@DOX NP after irradiation for 3 h. (B) UV-vis absorbance changes of PtAIECP@DOX NP with irradiation for different intervals. (C) Normalized UV-vis absorbance of PtAIECP@DOX NP at 298 nm under intermittent irradiation with different wavelengths. (D) Particle size changes of PtAIECP NP and PtAIECP@DOX NP with irradiation. (E) X-ray photoelectron spectroscopy (XPS) spectrum change of PtAIECP NP with irradiation for 3 h. (F) GPC curve change of PtAIECP NP with irradiation for 3 h. (G) Pt and DOX release profiles of PtAIECP@DOX NP in different irradiation conditions. Light source: visible light (500 nm, 20 mW/cm²).

PBS three times, followed by pancreatin digestion. After cell counting, the cells were lysed by lysis buffer (200 μ L, diluted three times with PBS) and further for Pt concentration determination by inductively coupled plasma mass spectrometry (ICP-MS). For the determination of Pt-DNA adducts, the cells were washed with PBS three times, followed by lysing with lysis buffer (200 μ L, diluted three times with PBS); then, the DNA amount was determined by DNA assay kit, and the Pt concentration was determined by ICP-MS.

2.8. MTT Assay and Combination Index (CI) Analysis.

Evaluation of cytotoxicity by MTT assay and analysis of CI are described in detail in the Supporting Information according to previous refs^{16, 44, 45}.

2.9. JC-1 Assay.

Skov-3 cells (5×10^4 /per well) were seeded into six-well plates and incubated for 24 h. The cells were then treated with AIECP NP or PtAIECP NP with a TPE content of 30 μ g at 37 $^{\circ}$ C.

After 4 h, one group was exposed to irradiation (500 nm, 20 mW/cm²) for 30 min and the other group was kept in the dark. A solution of JC-1 reagent (10 μ g/mL in medium) was added and incubation was carried out at 37 $^{\circ}$ C for 30 min. The cells were washed with PBS three times, fixed in 4% paraformaldehyde, and mounted onto glass slides for visualization by the CLSM system.

2.10. Cell Apoptosis. Evaluation of cell apoptosis by flow cytometry is described in detail in the Supporting Information according to previous ref 16.

2.11. Animal Tumor Model Establishment. BALB/c nude mice (male, 5–6 weeks old, \sim 20 g) were purchased from Jilin University (Changchun, China). All animals were maintained under required conditions and had free access to food and water throughout the experiments. The BALB/c nude mice bearing subcutaneous Skov3 and Skov3/RFP tumor models were developed by the subcutaneous

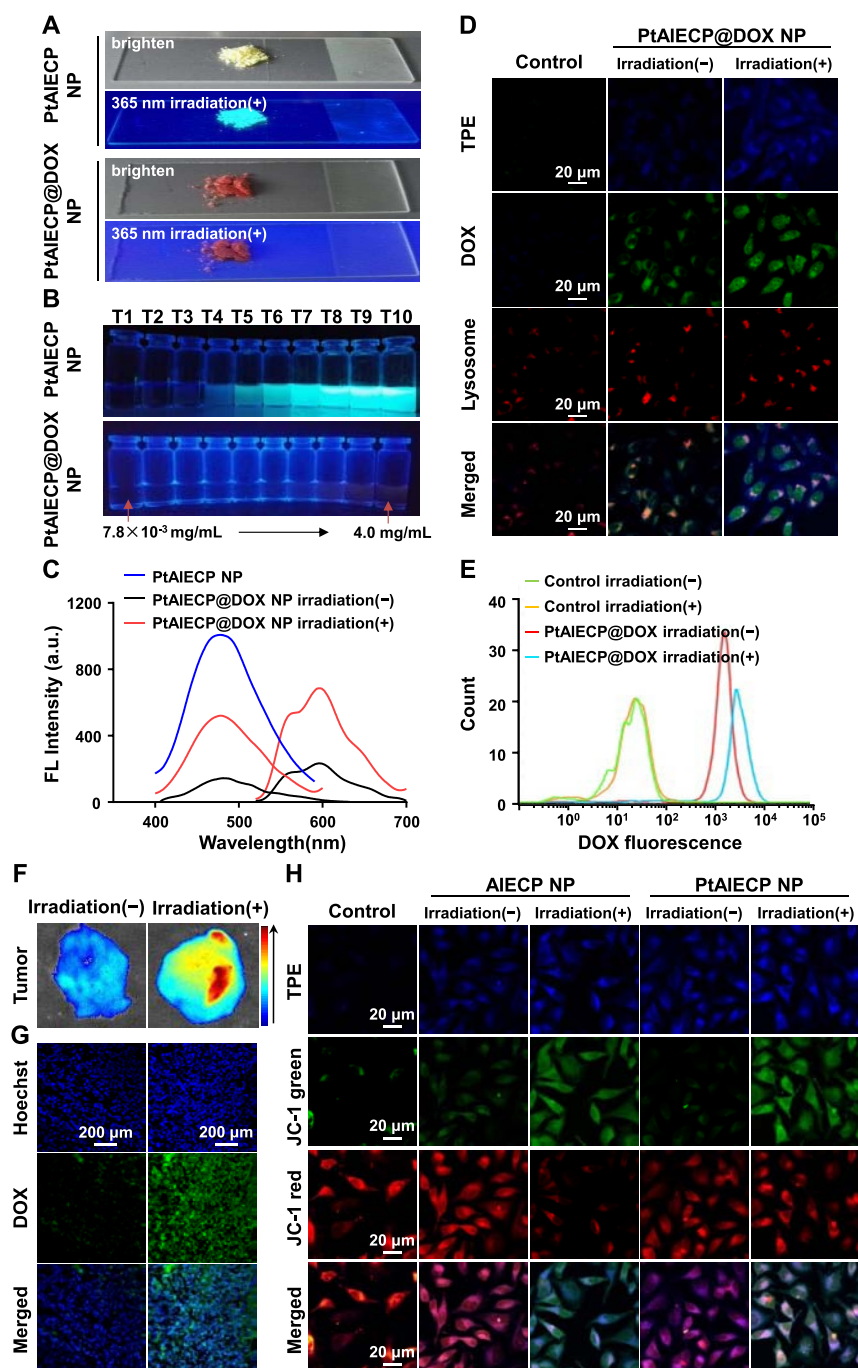


Figure 2. PtAIECP@DOX NP for dual-drug monitoring in vitro and ex vivo. (A) Aggregation-induced emission of PtAIECP NP and PtAIECP@DOX NP powders under room light and UV irradiation (365 nm). (B) Aggregation-induced emission of PtAIECP NP and PtAIECP@DOX NP aqueous solutions with various concentrations under UV irradiation (365 nm). (C) Fluorescence spectra of PtAIECP NP and PtAIECP@DOX NP with or without light irradiation. (D) CLSM images of Skov3 cells after treatment with PtAIECP@DOX NP with or without light irradiation. (E) The DOX fluorescence of Skov3 cells treated with PtAIECP@DOX for 24 h measured by flow cytometry. (F) Ex vivo DOX fluorescence of tumor tissues and (G) tumor tissue sections after intravenous injection of PtAIECP@DOX NP for 24 h with or without light irradiation. (H) Cellular level JC-1 assay by CLSM imaging. Light source: visible light (500 nm, 20 mW/cm²).

injection of Skov3 and Skov3/RFP cells (5×10^6 cells) to the right leg of the mice, respectively. The use of animals for this study was approved by the Animal Ethics Committee of Changchun Institute of Applied Chemistry, Chinese Academy of Sciences.

2.12. Biodistribution of DOX. Mice bearing subcutaneous Skov3 tumor model with a tumor volume of ~ 100 mm³ were randomly divided into 2 groups. Next, PtAIECP@DOX NP (2.5 mg Pt/kg, 3.125 mg DOX/kg) was injected intravenously away from light. One group was exposed to light irradiation (500 nm, 20 mW/cm²) for 30

min at the tumor site after 24 h, while the other group was maintained in the dark all the time. Then, the tumors were excised for ex vivo fluorescence imaging, followed by fixing with 4% formaldehyde and embedding in paraffin. Then, the tissues were cut into slices at a thickness of 2 μm and stained with Hoechst for the observation using the CLSM system.

2.13. Antitumor Efficacy. Mice bearing subcutaneous Skov3/RFP tumor model with a tumor volume of ~ 100 mm³ were randomly divided into 5 groups, and the initial weight and tumor volume were

recorded. Next, saline, cisplatin (2.5 mg Pt/kg, $n = 5$), DOX (3.125 mg DOX/kg, $n = 5$), PtAIECP NP (2.5 mg Pt/kg, $n = 10$), and PtAIECP@DOX NP (2.5 mg Pt/kg, 3.125 mg DOX/kg, $n = 10$) were injected intravenously on day 0, 3, and 6 away from light. Then, the mice treated with PtAIECP NP and PtAIECP@DOX NP were further randomly divided into two groups. One group was exposed to light irradiation (500 nm, 20 mW/cm²) for 30 min at the tumor site on day 1, 4, and 7, while the other group was maintained in the dark. Mice treated with saline, cisplatin, and DOX were also constantly maintained in the dark. Tumor volume was measured every 3 days and further calculated by the following equation: tumor volume = length \times width \times width/2. During the treatment, from day 0, all mice were anesthetized with 10% chloral hydrate every week for *in vivo* RFP fluorescence imaging. At the end of the experiment, the tumors were excised for *ex vivo* RFP fluorescence imaging.

2.14. Histological Analysis. The major tissues and tumors were excised at the end of the antitumor efficacy experiment, followed by fixing with 4% formaldehyde and embedding in paraffin. Then, the tissues were cut into slices of 2 μ m thickness for H&E and Tunnel. Then, the stained samples were observed by microscope and CLSM.

2.15. Statistical Analysis. Data were presented as the mean \pm standard deviation. The statistical significance was carried out and defined using analysis of variance test and two-tailed Student's *t* test as follows: * $p < 0.05$, ** $p < 0.01$, *** $p < 0.001$.

3. RESULTS AND DISCUSSION

Scheme 1 shows the structure of an amphiphilic ABA triblock copolymer containing photoactivatable Pt(IV) prodrug and aggregation-induced emission on the backbone (PtAIECP). The end block A is water-soluble PEG_{2k} (2000 g/mol) and the middle block B is hydrophobic polyurethane-urea with repeating units of photoactivatable Pt(IV) prodrug and AIEgen TPE. The photocleavable polyurethane-urea block was first prepared by the step-growth polymerization of biocompatible LDI-terminated Pt(IV) with a slight excess of TPE-N and then reacted with alkyne-terminated PEG_{2k} through spontaneous amino-yne click reaction to yield a triblock copolymer PtAIECP (Figures S1–S3).⁴⁷ The successful synthesis of PtAIECP was confirmed by ¹H NMR and FTIR (Figures S4 and S5). The molecular weight (M_n) was measured to be 9600 g/mol by gel permeation chromatography (GPC) (Figure 1E), and the degree of polymerization was determined to be 4 by ICP-MS, which agrees with the ¹H NMR result. The PtAIECP-assembled nanoparticles (PtAIECP NP) have an average hydrodynamic diameter of \sim 150 nm, as measured by DLS (Figure S6). The critical micelle concentration of PtAIECP was determined to be 1.24×10^{-2} mg/mL (Figure S7). Next, the ability of PtAIECP NP to encapsulate hydrophobic anticancer DOX was studied. The DMSO mixed solution of DOX and PtAIECP was added dropwise into the aqueous solution to prepare PtAIECP@DOX NP, and the DOX encapsulating ability in NP was studied. The content of Pt in PtAIECP remains unchanged because the polymerization degree of the Pt(IV) prodrug is fixed. The DOX-loading efficiency and the Pt/DOX ratio could be regulated by changing the feeding amount of DOX (Figure S7D). The final drug-loading contents of Pt and DOX in PtAIECP@DOX NP used for the following experiments were 10.4 and 13.0 wt %, respectively. The morphology of PtAIECP NP and PtAIECP@DOX NP were characterized by TEM and DLS. Spherical structure was observed for both nanoparticles, indicating their micellar morphology (Figure 1A). According to the DLS results, the hydrodynamic size of PtAIECP@DOX NP decreased after the loading of DOX due to the π - π interaction of TPE and DOX (Figure S6).

Next, we investigated the light activation of Pt(IV) in the PtAIECP backbone. The departure of azide ligands from Pt(IV) after irradiation could be detected by UV-vis absorption spectroscopy by the decrease in the absorbance at 298 nm. We monitored the UV-vis absorption change of PtAIECP@DOX NP under light irradiation at three different wavelengths (365, 430, and 500 nm) with the light intensity being fixed at 20 mW/cm². As shown in Figure 1B, the absorption at 298 nm declined steadily under continuous light irradiation (Figure S8). PtAIECP@DOX NP displayed the fastest degradation rate under 365 nm light and was fully dissociated within only 1 h, indicating the rapid conversion of Pt(IV) into Pt(II). Although the dissociation was slowest at 500 nm, the complete dissociation could still be achieved within 3 h. These results reveal that PtAIECP@DOX NP retained the light responsiveness while the absorption wavelength extends to green light (500 nm). When pulsed irradiation was applied, the absorption at 298 nm of PtAIECP@DOX NP displayed an ON/OFF effect (Figure 2C). Irregular and smaller nanoparticles also appeared under TEM, with the size distribution significantly changed (Figure 1A,D). Furthermore, X-ray photoelectron spectroscopy (XPS) was used to identify the oxidation state of Pt in PtAIECP NP (Figure 1E). The Pt 4f peaks in PtAIECP NP exhibited the binding energies of 77.9 and 74.7 eV before irradiation, which were changed to 76.5 and 72.8 eV, respectively, after irradiation, indicating the reduction-activation of Pt(IV) to Pt(II) in PtAIECP NP after irradiation. Additionally, the retention time in GPC curves changed significantly from 14 to 20 min and a multimodal distribution appeared after light irradiation (Figure 1F), demonstrating the light dissociation of the PtAIECP backbone, which would further lead to light-induced release of both activated Pt(II) and DOX. We simulated the internal pH environment in the tumor site to examine the drug release of PtAIECP@DOX NP *in vitro*. With pre-irradiation, more than 30% of Pt and DOX were released rapidly from PtAIECP@DOX NP in the first hour, while negligible release was detected under dark (Figure S9A,B). Contrary to the dark condition, PtAIECP@DOX NP showed a sustained release under continuous light irradiation (Figure 1G). During intermittent irradiation, drug release continued to increase in the irradiation stage, while no release was observed in the dark, displaying a switch ON/OFF effect (Figure S9C,D).

As shown in Figure 2A, both PtAIECP NP and PtAIECP@DOX NP had no fluorescence under sunlight in solid state. Upon light irradiation at 365 nm, PtAIECP NP powder emitted strong fluorescence, while PtAIECP@DOX NP powder did not. Figure 2B displays the photograph of the aqueous solutions of the polymer NPs under UV lamp. The luminescence phenomenon of aqueous solutions was similar to that of powders. Green fluorescence was observed in PtAIECP NP solution, and the intensity increased with increasing polymer concentration, while PtAIECP@DOX NP was barely fluorescent in water. The fluorescence spectra of PtAIECP@DOX NP and PtAIECP NP solutions at different excitation wavelengths were compared (Figure 2C). When PtAIECP@DOX NP was excited at 330 nm, no obvious fluorescence at 480 nm for TPE was observed, while PtAIECP NP expressed intense fluorescence at the same concentration. These results indicate that the fluorescence energy from TPE was effectively absorbed by DOX. Upon excitation at 488 nm, PtAIECP@DOX NP still showed emission signal at 591 nm for DOX, but

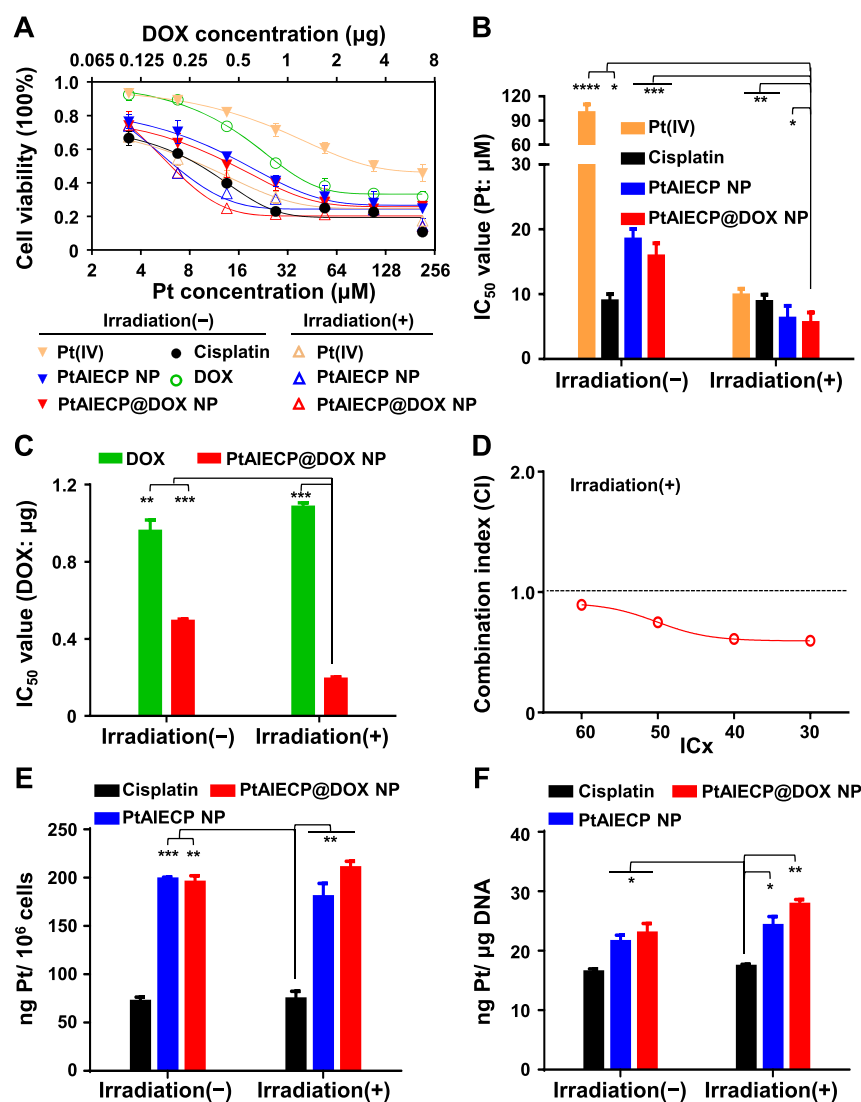


Figure 3. In vitro light-activatable combination efficacy and mechanism of PtAIECP@DOX NP against Skov3 cells. (A) Cell viability curves of Skov3 cells. (B) IC_{50} values of cisplatin, Pt(IV), PtAIECP NP, and PtAIECP@DOX NP ($\mu\text{M}/\text{Pt}$) against Skov3 cells after 72 h of incubation with or without irradiation. (C) IC_{50} values of DOX and PtAIECP@DOX NP ($\mu\text{g}/\text{DOX}$) against Skov3 cells after 72 h of incubation with or without irradiation. (D) CI curve of Pt and DOX in PtAIECP@DOX NP at 72 h with irradiation. (E) Cellular Pt uptake and (F) Pt-DNA adducts after 4 h incubation of drugs. Light source: visible light (500 nm, 20 mW/cm^2).

the fluorescence was partially quenched compared with that of pure DOX due to the π - π stacking of TPE and DOX's rigid planar aromatic rings. The fluorescent intensity difference could be utilized for monitoring the light activation of the Pt(IV) prodrug and the light-induced release of Pt(II) and DOX. When PtAIECP@DOX NP was exposed to irradiation, the Pt(IV) prodrug in the polymer backbone was reduction-activated to active Pt(II), inducing the dissociation of the nanoparticles and release of DOX. Therefore, the fluorescence of TPE was restored because the FERT effect between TPE and DOX was destroyed, and the fluorescent intensity of DOX was also strengthened because of the reduction of ACQ effect after the release of encapsulated DOX (Figure 2C). Furthermore, the dual-color fluorescence monitoring of PtAIECP@DOX NP in cancer cells was investigated by CLSM. After incubation with Skov3 cells in the dark, compared with PtAIECP NP sample, for PtAIECP@DOX NP sample, very weak blue fluorescence from TPE and green fluorescence from DOX were observed in cytoplasm (Figure

2D). However, the blue fluorescence in cytoplasm was significantly enhanced after light irradiation, and the green fluorescence diffused into the cell nucleus. The same phenomenon was also observed in the flow cytometry (Figure 2E). These results suggest that the integrity of PtAIECP@DOX NP was maintained under dark. However, upon light irradiation, the micelles began to dissociate, resulting in the appearance of blue fluorescence (from TPE) and the enhancement of green fluorescence (from DOX). By monitoring the spatiotemporal change of different fluorescent signals of PtAIECP@DOX NP, it was apparent that after endocytosis by endo/lysosomes, PtAIECP@DOX NP was transported into the cytoplasm where prodrugs were activated to release Pt(II) and DOX, which were then gradually diffused into the cell nucleus. Furthermore, the ex vivo fluorescence imaging of the tumor tissues and tumor tissue sections after the intravenous injection of PtAIECP@DOX NP for 24 h with or without light irradiation were performed. As shown in Figure 2F,G, the DOX fluorescence in the tumor tissue was barely

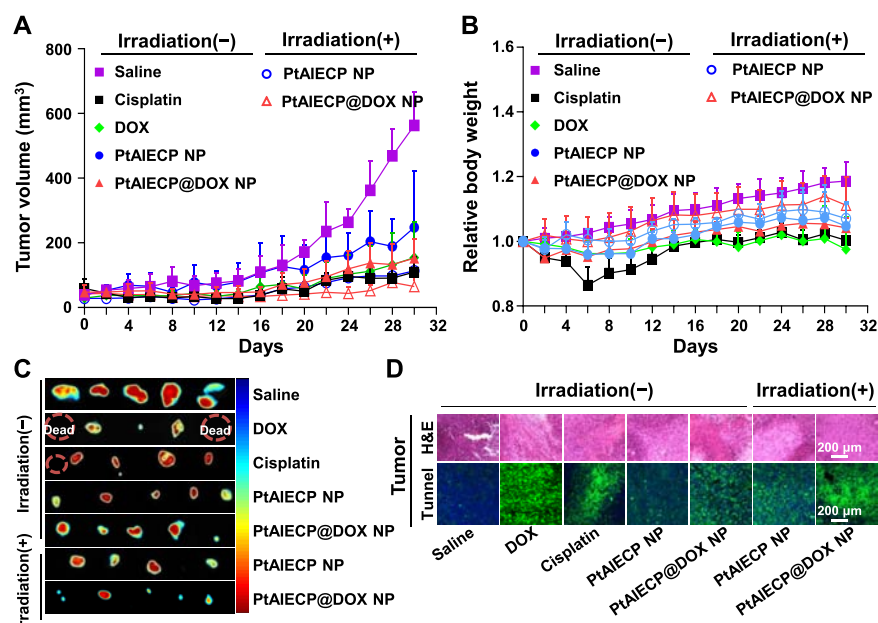


Figure 4. In vivo light-activatable combinational antitumor efficacy and mechanism of PtAIECP@DOX NP. A subcutaneous Skov3/RFP tumor model was established. (A) Tumor growth inhibition curves and (B) body weight tracing of mice during different treatments. (C) Ex vivo RFP fluorescence imaging of tumor at the end of the treatment. (D) Immunofluorescence examination of TUNEL examination and H&E staining of tumor tissues at the end of the treatment.

found without light irradiation, while strong fluorescence was observed after irradiation due to the Pt(IV) prodrug light-activation-induced dissociation of PtAIECP@DOX NP and release of encapsulated DOX.

It is reported that TPE would compromise the mitochondrial membrane, inducing the mitochondrial dysfunction of cancer cells.⁴⁸ The change in the mitochondrial transmembrane potential of Skov3 cells before and after PtAIECP NP treatment was examined by JC-1 staining (Figure 2H). In normal cells, JC-1 could convert to the aggregated form and would exhibit red fluorescence in mitochondria above a critical concentration. In contrast, JC-1 would not accumulate in mitochondria and remains as a green fluorescent monomer in the cytoplasm in apoptotic cells. Under light irradiation, similar to AIECP (copolymer without the Pt(IV) prodrug, Figure S10) NP treatment, mitochondrial membrane depolarization was detected by a shift from red to green in the fluorescence emission of JC-1 after PtAIECP NP treatment. Furthermore, after irradiation, the AIECP NP treated cells showed a significantly greater late apoptotic cell population (23.6%) than that of its dark control (7.60%), comparable to that of PtAIECP NP (26.7%) (Figure S11). These results demonstrate that TPE in PtAIECP NP may induce cancer cell apoptosis via mitochondrial dysfunction. The cytotoxicity of PtAIECP NP and PtAIECP@DOX NP against Skov3 cells was further evaluated by MTT assay. Higher cytotoxicity was observed for PtAIECP@DOX NP compared to cisplatin or DOX only (Figure 3A). After light irradiation, the IC_{50} values of cisplatin and DOX remained unchanged, suggesting that light was not conducive to cisplatin and DOX (Figure 3B,C). Compared with that of its counterparts in dark condition, the cytotoxicity of PtAIECP@DOX NP with light irradiation was significantly promoted. The IC_{50} value of PtAIECP@DOX NP ($5.66 \mu\text{m}/\text{Pt}$, $0.2 \mu\text{g}/\text{DOX}$) was much lower than that of cisplatin ($8.9 \mu\text{m}/\text{Pt}$) and DOX ($1.09 \mu\text{g}/\text{DOX}$). The synergistic effect of Pt and DOX of PtAIECP@DOX NP

with light irradiation was also evaluated by calculating the combination indexes (CI) (Figure 3D). Cisplatin and DOX can all serve as stand-alone regimens. The CI indexes of PtAIECP@DOX NP were calculated to be less than 1.0, indicating that the co-delivery of DOX and Pt(IV) in the same vehicle showed a synergistic effect with light stimulation.⁴³ To confirm the cancer cell killing mechanism, the cellular accumulation of Pt and Pt-DNA adducts were quantitatively determined by ICP-MS. Without irradiation, PtAIECP NP ($200 \pm 3.1 \text{ ng Pt}/10^6 \text{ cells}$) and PtAIECP@DOX NP ($190 \pm 6.2 \text{ ng Pt}/10^6 \text{ cells}$) exhibited ca. 3.5-fold higher accumulation in cells than cisplatin ($75.0 \pm 7.2 \text{ ng Pt}/10^6 \text{ cells}$), demonstrating an enhanced uptake of polymer NPs (Figure 3E). The amount of Pt-DNA adducts in the PtAIECP@DOX NP treated cells was the highest ($28.2 \pm 1.2 \text{ ng Pt}/\mu\text{g DNA}$) after irradiation (Figure 3F). All of the results indicate that light-activatable PtAIECP@DOX NP promoted the DNA platinization to induce synergistic cell apoptosis in vitro.

As we all know, Pt(II)-based anticancer drugs are the first-line drugs for ovarian cancer chemotherapy, and ovarian cancer is a kind of superficial cancer. Based on the excellent cytotoxicity of PtAIECP@DOX NP against Skov3 ovarian cancer cells, we further established a subcutaneous Skov3/RFP ovarian cancer model in nude mice, which can be penetrated by visible light (green light, 500 nm) to verify the antitumor effect in vivo.⁴⁹ The antitumor effect of PtAIECP@DOX NP was comparable to that of DOX and was lower than that of cisplatin in the dark, which was attributed to the high dark stability of copolymer NPs. In comparison, the antitumor efficiency of PtAIECP NP and PtAIECP@DOX NP was significantly improved under irradiation (Figure 4A). As observed from the tumor inhibition curves, PtAIECP@DOX NP with irradiation exhibited the best antitumor effect, which is better than that of cisplatin and PtAIECP NP, demonstrating that Pt and DOX actually exert excellent therapeutic effects in combination therapy (Figure S12). According to the ex vivo

tumor fluorescence images (Figures 4C and S13), the final tumor volume in PtAIECP@DOX NP in the irradiation group was the smallest and fluorescence intensity was much weaker, followed by the cisplatin group. To investigate the antitumor mechanism, H&E and TUNEL staining were performed on tumor tissue sections (Figure 4D). Significant necrosis and severe absence of nuclei were observed for H&E staining in the whole area of tumor section after PtAIECP@DOX NP treatment. TUNEL staining images also demonstrate that PtAIECP@DOX NP exhibited an obvious superiority on inducing apoptosis of tumor cells.⁵⁰ All of the results prove the synergistic antitumor effect of PtAIECP@DOX NP in vivo.

Furthermore, the body weights of mice were measured for safety evaluation (Figure 4B). The mice treated with cisplatin experienced significant body weight loss, and one mouse died on the 24th day, implying the severe systemic toxicity of cisplatin (Figure S14A). However, the copolymer groups showed much lower side effects on the mice, evidenced by their relatively stable health condition. Their body weights were constant throughout the experiment and no death occurred until the end of the experiment. To further evaluate the in vivo toxicity, the clinical blood parameters were measured. The levels of uric acid and creatinine of the mice treated with DOX and cisplatin were obviously higher than that of saline, PtAIECP NP, and PtAIECP@DOX NP (Figure S14B), indicating that those small molecular drugs had different degrees of damage to the liver and kidney functions. The results are consistent with the results of the biodistribution study and the H&E staining of normal organs. Pt accumulation in the liver, kidney, and spleen after cisplatin administration was higher than that of copolymer NPs groups (Figure S15). Compared with other groups, cisplatin induced noticeable signal of damage in renal area, with remarkable necrosis in proximal tubules and loss of brush border in renal tubules (Figure S14C). All of the results indicate that PtAIECP@DOX NP exhibited a safer and more effective cancer treatment performance.

4. CONCLUSIONS

We have developed a new light-activatable prodrug and aggregation-induced emission copolymer for dual-drug monitoring and combination chemotherapy. The obtained polyprodrug nanoparticles (PtAIECP@DOX NP) can respond to different wavelengths of light with a chain-cleavage scattered release of bioactive Pt(II) and DOX, simultaneously, leading to significant changes of fluorescence intensity. The in vitro and ex vivo results also demonstrate that the polyprodrug nanoparticles enabled monitoring of the light activation of the Pt(IV) prodrug into active Pt(II) drug and the release of encapsulated DOX. Besides, the combination of Pt(IV) and DOX showed synergistic anticancer effect in vitro and in vivo. The polyprodrug nanoparticle-based system possessing not only precisely controlled drug release behavior but also intrinsic ability to monitor prodrug activation and active drug release offers a new opportunity for the development of theranostic nanomedicine to maximize therapeutic benefits.

■ ASSOCIATED CONTENT

Supporting Information

The Supporting Information is available free of charge on the ACS Publications website at DOI: 10.1021/acsami.9b02346.

Materials and methods; synthesis and characterization of Pt(IV); synthesis and characterization of PtAIECP; FT-IR spectra of Pt(IV) and PtAIECP; Pt and DOX release profiles of PtAIECP@DOX NP in different conditions; synthesis and characterization of AIE copolymer; in vivo RFP fluorescence imaging of tumor during different treatments; bio-distribution of platinum (PDF)

■ AUTHOR INFORMATION

Corresponding Authors

*E-mail: yuzq@smu.edu.cn (Z.Y.).

*E-mail: ljz@jlu.edu.cn (J.L.).

*E-mail: east@ciac.ac.cn (D.Z.).

ORCID

Zhiqiang Yu: 0000-0002-1688-5558

Dongfang Zhou: 0000-0002-8381-7440

Author Contributions

[†]P.W. and X.W. contributed equally to this work.

Author Contributions

The manuscript was written through contributions of all authors.

Notes

The authors declare no competing financial interest.

■ ACKNOWLEDGMENTS

The authors would like to thank the financial support from National Natural Science Foundation of China (Nos. 51573069, 51773198, 51673188, and 81773642), Science and Technology Department of Jilin Province (No. 20170101091JC), Guangdong-Hong Kong Technology Cooperation Fund (No. 2017A050506016), and Open Research Fund of State Key Laboratory of Polymer Physics and Chemistry, Changchun Institute of Applied Chemistry, Chinese Academy of Sciences (No. 2018-24).

■ REFERENCES

- (1) Blanco, E.; Shen, H.; Ferrari, M. Principles of nanoparticle design for overcoming biological barriers to drug delivery. *Nat. Biotechnol.* **2015**, *33*, 941.
- (2) Xiao, H.; Yan, L.; Dempsey, E. M.; Song, W.; Qi, R.; Li, W.; Huang, Y.; Jing, X.; Zhou, D.; Ding, J.; Chen, X. Recent progress in polymer-based platinum drug delivery systems. *Prog. Polym. Sci.* **2018**, *87*, 70–106.
- (3) Gao, S.; Tang, G.; Hua, D.; Xiong, R.; Han, J.; Jiang, S.; Zhang, Q.; Huang, C. Stimuli-responsive bio-based polymeric systems and their applications. *J. Mater. Chem. B* **2019**, *7*, 709–729.
- (4) Pelaz, B.; Alexiou, C.; Alvarez-Puebla, R. A.; Alves, F.; Andrews, A. M.; Ashraf, S.; Balogh, L. P.; Ballerini, L.; Bestetti, A.; Brendel, C.; et al. Diverse applications of nanomedicine. *ACS Nano* **2017**, *11*, 2313–2381.
- (5) Yu, Y.; Xu, Q.; He, S.; Xiong, H.; Zhang, Q.; Xu, W.; Ricotta, V.; Bai, L.; Zhang, Q.; Yu, Z.; Ding, J.; Xiao, H.; Zhou, D. Recent advances in photosensitive metal-based drugs for drug delivery. *Coord. Chem. Rev.* **2019**, *387*, 154–179.
- (6) Shen, J.; Liu, H.; Mu, C.; Wolfram, J.; Zhang, W.; Kim, H.-C.; Zhu, G.; Hu, Z.; Ji, L.-N.; Liu, X.; Ferrari, M.; Mao, Z.-W.; Shen, H. Multi-step encapsulation of chemotherapy and gene silencing agents in functionalized mesoporous silica nanoparticles. *Nanoscale* **2017**, *9*, 5329–5341.
- (7) Wang, H.; Lu, Z.; Wang, L.; Guo, T.; Wu, J.; Li, Z.; Jiang, D.; Song, P.; Xie, H.; Zhou, L.; Xu, X.; Zheng, S.; et al. New generation nanomedicines constructed from self-assembling small-molecule prodrugs alleviate cancer drug toxicity. *Cancer Res.* **2017**, *77*, 6963–6974.

- (8) Ding, Q.; Xu, X.; Yue, Y.; Mei, C.; Huang, C.; Jiang, S.; Wu, Q.; Han, J. Nanocellulose-mediated electroconductive self-healing hydrogels with high strength, plasticity, viscoelasticity, stretchability, and biocompatibility toward multifunctional applications. *ACS Appl. Mater. Interfaces* **2018**, *10*, 27987–28002.
- (9) Kamaly, N.; Yameen, B.; Wu, J.; Farokhzad, O. C. Degradable controlled-release polymers and polymeric nanoparticles: Mechanisms of controlling drug release. *Chem. Rev.* **2016**, *116*, 2602–2663.
- (10) Zhen, X.; Xie, C.; Jiang, Y.; Ai, X.; Xing, B.; Pu, K. Semiconducting photothermal nanoagent for remote-controlled specific cancer therapy. *Nano Lett.* **2018**, *18*, 1498–1505.
- (11) Li, Y.; Song, L.; Lin, J.; Ma, J.; Pan, Z.; Zhang, Y.; Su, G.; Ye, S.; Luo, F.; Zhu, X.; Hou, Z. Programmed nanococktail based on pH-responsive function switch for self-synergistic tumor-targeting therapy. *ACS Appl. Mater. Interfaces* **2017**, *9*, 39127–39142.
- (12) Zhang, Y.; Yin, Q.; Yin, L.; Ma, L.; Tang, L.; Cheng, J. Chain-shattering polymeric therapeutics with on-demand drug-release capability. *Angew. Chem., Int. Ed.* **2013**, *52*, 6435–6439.
- (13) Yuan, Y.; Liu, J.; Liu, B. Conjugated-polyelectrolyte-based polyprodrug: Targeted and image-guided photodynamic and chemotherapy with on-demand drug release upon irradiation with a single light source. *Angew. Chem., Int. Ed.* **2014**, *126*, 7291–7296.
- (14) Guo, D.; Xu, S.; Huang, Y.; Jiang, H.; Yasen, W.; Wang, N.; Su, Y.; Qian, J.; Li, J.; Zhang, C.; Zhu, X. Platinum(IV) complex-based two-in-one polyprodrug for a combinatorial chemo-photodynamic therapy. *Biomaterials* **2018**, *177*, 67–77.
- (15) Zhou, D.; Guo, J.; Kim, G. B.; Li, J.; Chen, X.; Yang, J.; Huang, Y. Simultaneously photo-cleavable and activatable prodrug-backboned block copolymer micelles for precise anticancer drug delivery. *Adv. Healthcare Mater.* **2016**, *5*, 2493–2499.
- (16) He, S.; Li, C.; Zhang, Q.; Ding, J.; Liang, X. J.; Chen, X.; Xiao, H.; Chen, X.; Zhou, D.; Huang, Y. Tailoring platinum(IV) amphiphiles for self-targeting all-in-one assemblies as precise multimodal theranostic nanomedicine. *ACS Nano* **2018**, *12*, 7272–7281.
- (17) Cong, Y.; Xiao, H.; Xiong, H.; Wang, Z.; Ding, J.; Li, C.; Chen, X.; Liang, X.-J.; Zhou, D.; Huang, Y. Dual drug backboned shattering polymeric theranostic nanomedicine for synergistic eradication of patient-derived lung cancer. *Adv. Mater.* **2018**, *30*, No. 1706220.
- (18) Zhang, Z.; Wu, Y.; Kuang, G.; Liu, S.; Zhou, D.; Chen, X.; Jing, X.; Huang, Y. Pt(IV) prodrug-backboned micelle and DCA loaded nanofibers for enhanced local cancer treatment. *J. Mater. Chem. B* **2017**, *5*, 2115–2125.
- (19) Xu, X.; Saw, P. E.; Tao, W.; Li, Y.; Ji, X.; Bhasin, S.; Liu, Y.; Ayyash, D.; Rasmussen, J.; Huo, M.; Shi, J.; Farokhzad, O. C. ROS-responsive polyprodrug nanoparticles for triggered drug delivery and effective cancer therapy. *Adv. Mater.* **2017**, No. 1700141.
- (20) Wang, W.; Liang, G.; Zhang, W.; Xing, D.; Hu, X. Cascade-promoted photo-chemotherapy against resistant cancers by enzyme-responsive polyprodrug nanoplateforms. *Chem. Mater.* **2018**, *30*, 3486–3498.
- (21) Liow, S. S.; Dou, Q.; Kai, D.; Li, Z.; Sugiarto, S.; Yu, C. Y. Y.; Kwok, R. T. K.; Chen, X.; Wu, Y. L.; Ong, S. T.; Kizhakeyil, A.; Verma, N. K.; Tang, B. Z.; Loh, X. J. Long-term real-time in vivo drug release monitoring with AIE thermogelling polymer. *Small* **2017**, *13*, No. 1603404.
- (22) Miao, Q.; Pu, K. Organic semiconducting agents for deep-tissue molecular imaging: second near-infrared fluorescence, self-luminescence, and photoacoustics. *Adv. Mater.* **2018**, *30*, No. 1801778.
- (23) Miao, Q.; Xie, C.; Zhen, X.; Lyu, Y.; Duan, H.; Liu, X.; Jesse, V. J.; Pu, K. Molecular afterglow imaging with bright, biodegradable polymer nanoparticles. *Nat. Biotechnol.* **2017**, *35*, 1102–1110.
- (24) Liu, Z.; Chen, N.; Dong, C.; Li, W.; Guo, W.; Wang, H.; Wang, S.; Tan, J.; Tu, Y.; Chang, J. Facile construction of near infrared fluorescence nanoprobe with amphiphilic protein-polymer bioconjugate for targeted cell imaging. *ACS Appl. Mater. Interfaces* **2015**, *7*, 18997–19005.
- (25) He, S.; Song, J.; Qu, J.; Cheng, Z. Crucial breakthrough of second near-infrared biological window fluorophores: design and synthesis toward multimodal imaging and theranostics. *Chem. Rev.* **2018**, *47*, 4258–4278.
- (26) Li, N.; Chang, C.; Pan, W.; Tang, B. A multicolor nanoprobe for detection and imaging of tumor-related mRNAs in living cells. *Angew. Chem., Int. Ed.* **2012**, *51*, 7426–7430.
- (27) Zhao, N.; Lam, J. W. Y.; Sung, H. H. Y.; Su, H. M.; Williams, I. D.; Wong, K. S.; Tang, B. Z. Effect of the counterion on light emission: A displacement strategy to change the emission behaviour from aggregation-caused quenching to aggregation-induced emission and to construct sensitive fluorescent sensors for Hg²⁺ detection. *Chem. - Eur. J.* **2014**, *20*, 133–138.
- (28) Chen, G.; Li, W.; Zhou, T.; Peng, Q.; Zhai, D.; Li, H.; Yuan, W. Z.; Zhang, Y.; Tang, B. Z. Conjugation-induced rigidity in twisting molecules: Filling the gap between aggregation-caused quenching and aggregation-induced emission. *Adv. Mater.* **2015**, *27*, 4496–4501.
- (29) Hong, Y.; Lam, J. W.; Tang, B. Z. Aggregation-induced emission: phenomenon, mechanism and applications. *Chem. Commun.* **2009**, 4332–4353.
- (30) Kwok, R. T. K.; Leung, C. W. T.; Lam, J. W. Y.; Tang, B. Z. Biosensing by luminogens with aggregation-induced emission characteristics. *Chem. Soc. Rev.* **2015**, *44*, 4228–4238.
- (31) Wang, X.; Song, P.; Peng, L.; Tong, A.; Xiang, Y. Aggregation-induced emission luminogen-embedded silica nanoparticles containing DNA aptamers for targeted cell imaging. *ACS Appl. Mater. Interfaces* **2016**, *8*, 609–616.
- (32) Li, H.; Chang, J.; Hou, T.; Li, F. Aggregation induced emission amphiphile with an ultra low critical micelle concentration: fabrication, self assembling, and cell imaging. *J. Mater. Chem. B* **2016**, *4*, 198–201.
- (33) Zhang, C.; Jin, S.; Li, S.; Xue, X.; Liu, J.; Huang, Y.; Jiang, Y.; Chen, W. Q.; Zou, G.; Liang, X.-J. Imaging intracellular anticancer drug delivery by self-assembly micelles with aggregation-induced emission (AIE Micelles). *ACS Appl. Mater. Interfaces* **2014**, *6*, 5212–5220.
- (34) Yuan, Y.; Zhang, C.-J.; Liu, B. A photoactivatable AIE polymer for light-controlled gene delivery: Concurrent endo/lysosomal escape and DNA unpacking. *Angew. Chem., Int. Ed.* **2015**, *54*, 11419–11423.
- (35) Ding, D.; Kwok, R. T. K.; Yuan, Y.; Feng, G.; Tang, B. Z.; Liu, B. A fluorescent light-up nanoparticle probe with aggregation-induced emission characteristics and tumor-acidity responsiveness for targeted imaging and selective suppression of cancer cells. *Mater. Horiz.* **2015**, *2*, 100–105.
- (36) Mei, J.; Hong, Y.; Lam, J. W. Y.; Qin, A.; Tang, Y.; Tang, B. Z. Aggregation-induced emission: The whole is more brilliant than the parts. *Adv. Mater.* **2014**, *26*, 5429–5479.
- (37) Mei, J.; Leung, N. L. C.; Kwok, R. T. K.; Lam, J. W. Y.; Tang, B. Z. Aggregation-induced emission: Together we shine, united we soar! *Chem. Rev.* **2015**, *115*, 11718–11940.
- (38) Liu, J.; Chen, C.; Ji, S.; Liu, Q.; Ding, D.; Zhao, D.; Liu, B. Long wavelength excitable near-infrared fluorescent nanoparticles with aggregation-induced emission characteristics for image-guided tumor resection. *Chem. Sci.* **2017**, *8*, 2782–2789.
- (39) Yuan, Y.; Xu, S.; Cheng, X.; Cai, X.; Liu, B. Bioorthogonal turn-on probe based on aggregation-induced emission characteristics for cancer cell imaging and ablation. *Angew. Chem., Int. Ed.* **2016**, *55*, 6457–6461.
- (40) Housman, G.; Byler, S.; Heerboth, S.; Lapinska, K.; Longacre, M.; Snyder, N.; Sarkar, S. Drug resistance in cancer: an overview. *Cancers* **2014**, *6*, 1769–1792.
- (41) Wu, Y.; Zhou, D.; Zhang, Q.; Xie, Z.; Chen, X.; Jing, X.; Huang, Y. Dual-sensitive charge-conversional polymeric prodrug for efficient codelivery of demethylcantharidin and doxorubicin. *Biomacromolecules* **2016**, *17*, 2650–2661.
- (42) Li, Y.; Lin, J.; Ma, J.; Song, L.; Lin, H.; Tang, B.; Chen, D.; Su, G.; Ye, S.; Zhu, X.; Luo, F.; Hou, Z. Methotrexate-camptothecin prodrug nanoassemblies as a versatile nanoplateform for biomodal imaging-guided self-active targeted and synergistic chemotherapy. *ACS Appl. Mater. Interfaces* **2017**, *9*, 34650–34665.

(43) Chen, Q.; Yang, Y.; Lin, X.; Ma, W.; Chen, G.; Li, W.; Wang, X.; Yu, Z. Platinum(IV) prodrugs with long lipid chains for drug delivery and overcoming cisplatin resistance. *Chem. Commun.* **2018**, *54*, 5369–5372.

(44) He, S.; Cong, Y.; Zhou, D.; Li, J.; Xie, Z.; Chen, X.; Jing, X.; Huang, Y. A dextran–platinum(IV) conjugate as a reduction-responsive carrier for triggered drug release. *J. Mater. Chem. B* **2015**, *3*, 8203–8211.

(45) Wu, P.; Zhou, D.; Huang, Y.; Li, J. Light-stimulus dual-drug responsive nanoparticles for photoactivated therapy using mesoporous silica nanospheres. *Chem. Res. Chin. Univ.* **2018**, *34*, 676–683.

(46) Lv, D.; Wang, R.; Tang, G.; Mou, Z.; Lei, J.; Han, J.; De Smedt, S. C.; Xiong, R.; Huang, C. Eco-friendly electrospun membranes loaded with visible-light response nano-particles for multifunctional usages: high-efficient air Filtration, dye scavenger and bactericide. *ACS Appl. Mater. Interfaces* **2019**, 12880–12889.

(47) He, B.; Su, H.; Bai, T.; Wu, Y.; Li, S.; Gao, M.; Hu, R.; Zhao, Z.; Qin, A.; Ling, J.; Tang, B. Z. Spontaneous amino-yne click polymerization: A powerful tool toward regio- and stereospecific poly(beta-aminoacrylate)s. *J. Am. Chem. Soc.* **2017**, *139*, 5437–5443.

(48) Shin, W. S.; Park, S. K.; Verwilt, P.; Koo, S.; Lee, J. H.; Chi, S. G.; Kim, J. S. Targeted combinational therapy inducing mitochondrial dysfunction. *Chem. Commun.* **2017**, *53*, 1281–1284.

(49) Sun, W.; Thiramanas, R.; Slep, L. D.; Zeng, X.; Mail-nder, V.; Wu, S. Photoactivation of anticancer Ru complexes in deep tissue: how deep can we go? *Chem. - Eur. J.* **2017**, *23*, 10832–10837.

(50) Zhang, Z.; Kuang, G.; Zong, S.; Liu, S.; Xiao, H.; Chen, X.; Zhou, D.; Huang, Y. Sandwich-like fibers/sponge composite combining chemotherapy and hemostasis for efficient post-operative prevention of tumor recurrence and metastasis. *Adv. Mater.* **2018**, *30*, No. 1803217.